8th International Conference
on
Wind Turbine Noise
Lisbon – 12th to 14th June 2019

Towards digital wind turbine noise certification

Wouter van der Velden and Damiano Casalino
Dassault Systemes Deutschland GmbH, Curiestraße 4, 70563, Stuttgart, Germany
wouter.vandervelden@3ds.com

Summary

Flow and acoustic simulations are performed on the NM80 full-scale 3-bladed wind-turbine, tested during the DanAero campaign. SIMULIA PowerFLOW's Lattice Boltzmann Method is used to predict the turbulent-resolved unsteady flow around the full wind-turbine, yielding good results with reference data. The noise at certification position for several rotor revolutions is computed using an auralization technique from simulated flow data stored along a portion of the rotor revolution. The auralization process is based on a frequency-domain Ffowcs-Williams and Hawking noise spectrum computation from blade wall-pressure pressure fluctuations, taking into account ground reflection. Noise spectra at several azimuthal copies of the microphones are finally corrected to take into account blade-motion Doppler effects end atmospheric absorption and smoothly appended to recover the full rotor revolution. Significant cost reduction in simulation time is found with the new post-processing process, making the entire process suitable for industrial turn-around-times.

1. Introduction

Wind energy; the solution to deal with an increasingly recognized and critical challenge for mankind. In order to reduce greenhouse gases, the demand for renewable energy, such as wind energy, is growing and growing. A study from van den Berg [13] showed that noise, and in particular the swishing character of the noise, is one of the most annoying aspects for onshore wind turbines. To protect public health, governments apply strict noise regulations for both maximum, average and modulated

noise levels. Hence, noise constitutes as an important barrier for the widespread application of wind energy as many wind turbines must operate at reduced power, especially during the night when background noise levels are lower. This leads to a lower power output from the turbines, which will lead to an overall reduction of the annual energy production, finally resulting in a loss of revenue.

Therefore, when designing a wind-turbine, an important target to optimize the wind turbine efficiency is the blades shape. As the wind power is directly related to the exposed surface area, one market trend is to propose increased rotor size which has two consequences, among others. One is that prototyping becomes more expensive and more challenging to carry out. The other is that the flow-induced noise contribution keeps increasing and can be a significant source of annoyance for people living in a nearby community. Aerodynamic noise is related to the rotational speed, the presence of tower, the inflow properties, the blade tip design and the blade geometry. The latter is increasing in complexity, with the airfoil profile, chord, and twist distributions depending on the span location in order to trade-off aerodynamic efficiency and noise. The blade-tower interactions mostly impact the low frequencies, whereas the overall blade self-noise is responsible of the mid and high frequency content caused by the vortical flow past the blade tip, flow separation in the inner part of the blade, vortex shedding from a blunt trailing edge, and boundary-layer turbulent fluctuations passing by the trailing edge [2, 10]. Tip noise and blunt-trailing-edge noise can be prevented by a proper blade design. Flow separation noise may be significant in off-nominal conditions and can be also reduced by a proper aerodynamic design and by using vortex generators. Whereas, mitigating turbulent-boundary-layer-trailing edge noise (subsequently denoted as trailing edge noise), which is widely recognized as the dominant source of wind-turbine noise, is way more challenging.

The goal of this paper is to apply the knowledge gained airfoil trailing-edge noise prediction in wind-tunnel quasi two-dimensional conditions to a full three-dimensional rotating turbine. The full-scale 2.3 MW NM80 turbine used in the DanAero [9] measurement campaign is considered. One of the three blades of the turbine was specifically manufactured for this experiment and equipped with multiple sensors. The blade is a LM 38.8 m blade attached to the hub at a radius of 1.24 m from the rotor center. Therefore, the rotor radius at the blade tip is 40.04 m, which includes the pre-bend of the blades. A met mast located near the turbine was used to monitor atmospheric conditions.

In this paper, SIMULIA's PowerFLOW time-explicit, compressible and transient solver based on Lattice-Boltzmann Method (LBM) is used to predict the unsteady flow and acoustic near field around the NM80 wind turbine. When performing the numerical simulation, the full-scale geometry is truly rotated using a local rotating body-fixed reference frame method. This type of simulation implemented in LBM has been already used and validated across various rotating machinery applications.

The present study provides a detailed analysis of the aerodynamic quantities, such as surface pressure coefficient, force and momentum at a single wind speed. The noise at IEC 61400-11 certification position for several rotor revolutions is computed using an auralization technique from simulated flow data stored along a portion of the rotor revolution. The auralization process is based on a frequency-domain Ffowcs-Williams and Hawking noise spectrum computation from blade wall-pressure pressure fluctuations, taking into account ground reflection. Noise spectra at several azimuthal copies of the microphones are finally corrected to take into account blade-motion Doppler effects end atmospheric absorption and smoothly appended to recover the full rotor revolution.

2. Methodology

2.1. Lattice Boltzmann Method

The numerical solver, which is based on the Lattice Boltzmann Method (LBM) with a wall-modeled Very Large Eddy Simulation (VLES) model for turbulence [5, 6, 14, 15], is extensively used for a wide range of industrial applications. As relevant to the present study, the solver has been also used to simulate the noise of rotating machines like wind-turbines[11], helicopter rotors[12], installed aircraft propellers[1, 7] and turbofans[3, 4, 8].

Lattice-based methods are by nature explicit, transient and compressible, and are an alternative to traditional CFD methods based on the discretization of the Navier-Stokes equations and derived variations. The basic idea of LBM is to track the advection and collisions of fluid particles. Since the average number of particles in a representative volume of fluid far exceeds the compute power required to track them individually, the particles are grouped into a set of discrete i-directions. The computation follows the particle distribution function f_i which represents the number of particles in a unit of volume at a specific time and location moving with velocity c_i. As in statistical physics, the flow variables such as density and velocity are determined by taking the appropriate moments, i.e. summations over the set of discrete directions, of the particle distribution function.

For simulations of flows with arbitrary geometry rotating around a fixed axis, the 3-D dimensional computational domain is divided into an inner and an outer domain. The inner domain has a grid fixed with the rotating geometry so that the geometry does not have a relative motion with respect to the grid. This forms a “body-fixed” Local Reference Frame (LRF) domain with the rotating geometry. The grid in the outer domain is fixed with the ground and forms a “ground-fixed” reference frame domain. The inner and outer domains are connected by a closed, zero-thickness, transparent interface.

Due to the unique properties of PowerFLOW, which is intrinsically unsteady and compressible, the acoustic pressure field can be extracted directly from the computational domain. For the far-field noise prediction, an additional set of tools is used, as described in next sub-section.

2.2. Acoustic certification prediction model

The main source of wind-turbine noise is the blade trailing edge, and in particular the outer part of it due to the higher velocity. The characteristic frequency ranges of trailing-edge noise scales as the flow velocity divided by the integral length of the turbulent flow fluctuations in the boundary layer. A more rigorous dimensional analysis is not need to argue that a large scale separation between noise frequencies and rotational frequency exists. Therefore, the noise computed in a blade-rotating reference system reaches a statistical convergence in a portion of the rotor revolution. This argument is used to develop an analysis process that allows to recover accurate noise signals over several rotor revolutions by using a CFD simulation covering only a small portion of the rotor revolution. The simple trick used in the process is to reproduce the different noise levels measured by a ground-fixed microphone during one rotor revolution by computing the noise levels at several microphones distributed along a ring coaxial with the wind-turbine. Since no relative motion between microphones and blade occurs, an efficient implementation of the Ffowcs-Williams and Hawkings (FW-H) formulation in the frequency domain can be used. Ground reflection is taken into account in exact way through a mirroring technique directly implemented in the FW-H integration process.

A reflection coefficient can be prescribed in order to take into account acoustic absorption without phase variations.

Since the different blades generate the same noise levels at the same relative positions, another way to reduce the computational cost of the full wind-turbine noise computation is to resolve the boundary-layer turbulent fluctuations with a fine mesh only in the outer part of one blade. The FW-H surface integration is applied to this blade portion and finally the noise from the full turbine is computed by adding signals properly shifted in time.

The FW-H computation generates spectra at different azimuthal locations. The amplitude variation over time for every single narrow band is then used to generate a synthetic noise signals using a standard auralization technique. Since the phase of the signal for every band and blade is generated randomly, several rotor revolutions can be reproduced. Prior auralization, a blade-rotation Doppler correction is applied by considering a source located at $0.8R_t$ (80% outboard). The same source location is used to compute the atmospheric absorption as a function of source/microphone distance and frequency.

For the sake of the present analysis, a full ground reflection is considered (no absorption). A number of 72 azimuthal microphones are used to recover a full rotor revolution. The physical ground-fixed microphones are located at 100 m downwind position, as indicated by the IEC 61400-11 process. A schematic of the microphones is added to Figure 1. An atmospheric humidity of 70% is considered. Noise signals are auralized along 5 rotor revolutions. The final noise spectra are computed by using about 1500 Welch windows with 50% overlap applied to the whole signals. The resulting frequency range is approximately $30 - 8,000$ Hz.

3. Wind turbine geometry and computational setup

The horizontal axis wind turbine used in current study is extracted (by best means) from the DanAero experimental campaign. The NM80 turbine is a 2.3 MW, full scale three bladed turbine, with LM Wind Power 38.8 m mounted blades. Detailed tower, hub and nacelle geometries are not available in the benchmark definition, and are replaced, for the sake of the present study, by realistic/arbitrary wind turbine geometries.

In the computations, the full turbine system is modeled without any geometrical simplification. The blades are pre-bended and attached to a default hub with a 1.24 m offset from the rotor center, resulting in a total length of $R = 40.04$ m. Furthermore, they were pitched 5 degrees towards lower angles of attack and tilted 2.5 degrees towards the pressure side to have the correct default pitch and rotor cone angle respectively. The rotor center is 59.89 m above ground, and the nacelle encapsulates a box with dimensions of $12 \times 4 \times 4$ meter. The tower is modeled as a tapered cylinder with 2.1 m at the base and 1.25 m at the top. An overview can be found in Figure 2, including the ground-fixed coordinate system.

The full geometry is embedded and centered into a large simulation domain of $100R \times 100R \times 100R$ to mimic free-field conditions. The floor is modeled as a standard rigid wall, while the ceiling is modeled as a frictionless wall to avoid the development of a boundary layer. All other boundary conditions are appropriately set as inlet/outlet conditions. Acoustic sponge zones in outer regions provide an anechoic condition to prevent spurious reflections of acoustic waves propagating from the wind turbine to the far field.

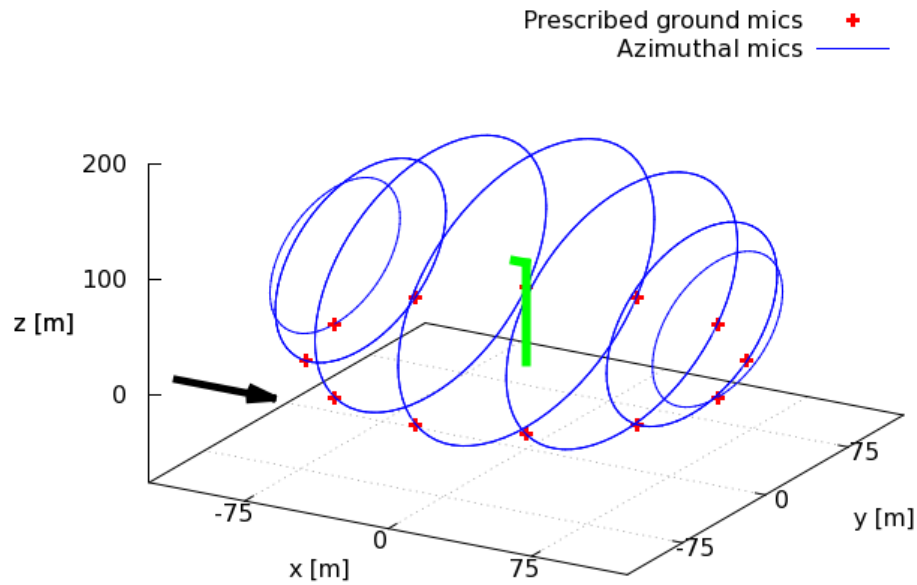

Fig. 1 Sketch of the ground microphone positions (red) and their azimuthal wind turbine axis rotating microphones (blue). Green indicates the turbine tower and nacelle, the arrow the wind direction

The grid generation process is fully automated and follows a user defined grid resolution scheme in regions of interest. The initial aerodynamic simulation is for converging and settling the rotor slipstream and the correct inflow around the blade. Highest resolution is placed around the outer 20 m part of a blade, ensuring local $y+$ values at the trailing edge do not exceed 80. The converged aerodynamic solution is then seeded onto an aeroacoustic simulation, which has an extra resolution to cover the transition strip, the resulting turbulent boundary layer, trailing edge and serrations. This results in a $y+$ value of 15 at inboard and 20 at outboard sections, or 0.45 mm, or 3200 voxels/grid cells along the average chord (1.5 m for the outer 20 m section). Details of the current resolution strategy are depicted in Fig 2. Transition location is variable along the blade span and extracted using the laminar-to-turbulent transition (LTT) model in aerodynamic modality in PowerFLOW, and cross-checked with XFOIL computations.

The simulation initial and boundary conditions are tried to be set as prescribed by the DanAero Task 39 1.1 case. This yields rigid construction (no deformation of the blades), no tilt, no tower shadow, no wind shear and no yaw angle error. The rotor speed is 12.3 RPM and the blades are pitched 0.15 degrees to the feather. A wind speed of $u_\infty = 6.1$ m/s is considered under standard atmospheric conditions ($\rho_\infty = 1.231$ kg/m^3 and $T_\infty = 19°$ C). As the prescribed atmospheric turbulence parameters in Task 39 are unrealistic for full scale CFD computations (long settling time and domain needed), standard turbulence parameters of $TI = 5$ % and $TL = 0.01$ m are used. This will have negligible effect on the aeroacoustic prediction, as the main goal of the present study is to evaluate trailing edge,

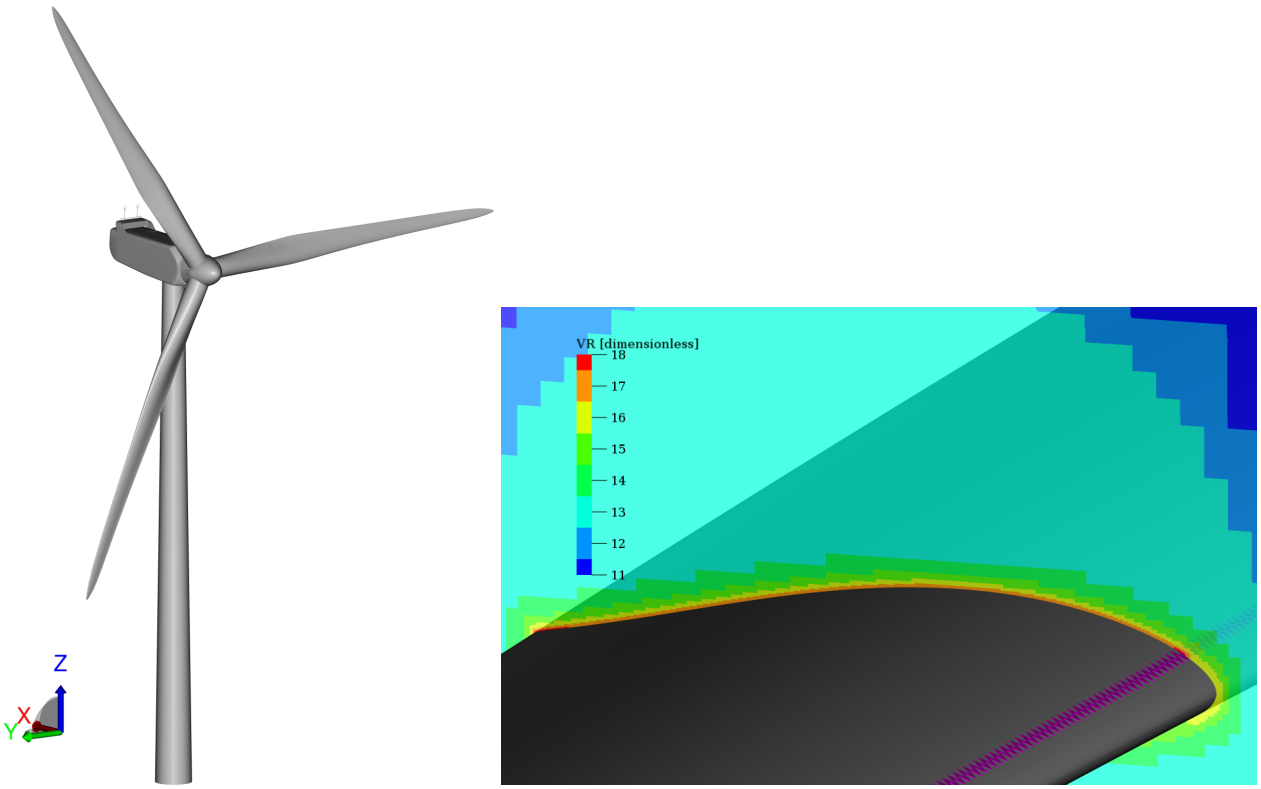

Fig. 2 Overview of the NM80 wind turbine geometry and close-up of the different refinement regions close to the blade

tip and stall noise. With these conditions, transition strips are placed around 6 % and 40 % of the suction and pressure side respectively.

As the aeroacoustic post-processing is optimally designed to handle large rotors under low RPM's, it is not required to run the aeroacoustic simulations for multiple revolutions to collect a 10 second bandwidth as stated by the IEC certification. Instead, only $1/12$th of the full revolution is modeled, i.e. 0.45 seconds. Together with an optimized setup of less than 300 million fine equivalent voxels (700 million overall), the user only need 85 kCPUh (i.e. < 3 days computation time on SIMULIA cloud) to obtain enough unsteady surface pressure data for the acoustic computation.

4. Results

The results are spitted into two section. Firstly, an overview of the aerodynamic performance is given, both qualitatively and quantitatively. Details of the unsteady velocity and pressure field give indication of the quality of the simulation, and of the quality of the certification noise prediction. The latter is discussed in the final section, detailing step by step the new certification noise process.

4.1. Aerodynamic information

To highlight the unsteadiness of the simulation, it is useful to observe and identify local separation at the root section of the blade. Therefore, in Figure 3, iso-λ_2 surfaces, colored by velocity magnitude are plotted. It can be observed that there is 1) a clear tip vortex present and 2) locally the flow separates

at $1/4$th of the inboard section of the blade. Fully attached flow is therefore expected at the outboard sections of this turbine, under the current simulated conditions. The fact that no turbulence seems to convect at the trailing edges of the outboard section of the blade, is due to the fact that this results originates from the aerodynamic settling part of the simulation. No transition strip was modeled here, and $y+$ values are relatively coarse.

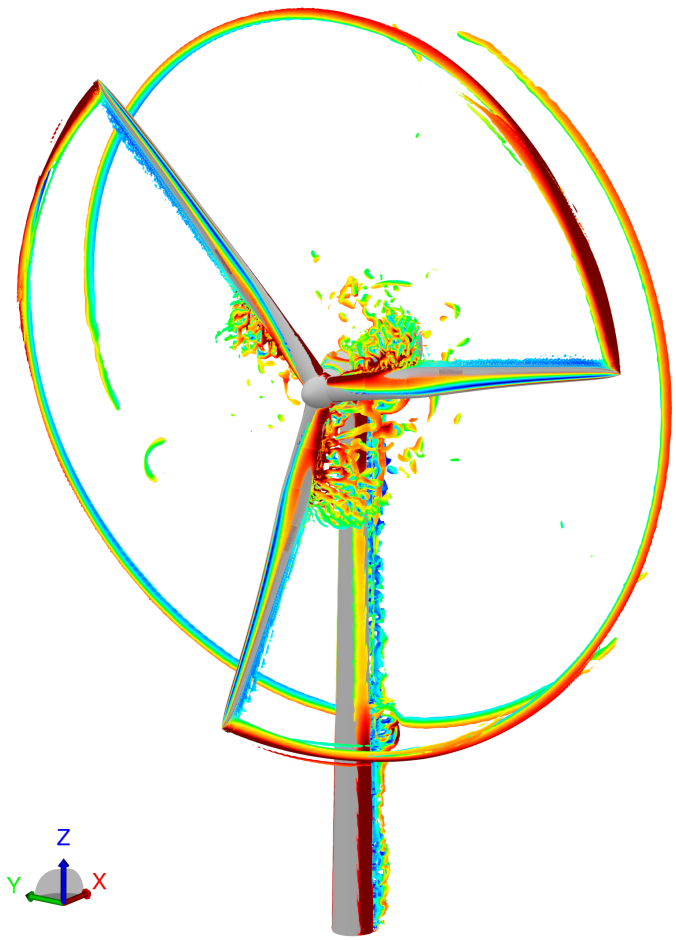

Fig. 3 Instantaneous snapshot of isosurfaces of λ_2, colored by velocity magnitude, extracted from the aerodynamic simulation

However, the simulation requirements of the aerodynamic simulation are sufficient enough to extract the mean quantities of the flow, such as the pressure distribution along different radial sections. In Figure 4, three spanwise locations are shown for which pressure data is extracted. A correlation with XFOIL 2-D results is made to cross-check the simulation results, showing good agreement. As expected, the largest pressure forces are obtained at midboard sections of the wing, where the flow is fully attached.

The aerodynamic generated noise studied in this paper is mainly affected by the turbulent boundary layer, convected past the trailing edge. Therefore, to have an idea of the type of turbulent flow, at

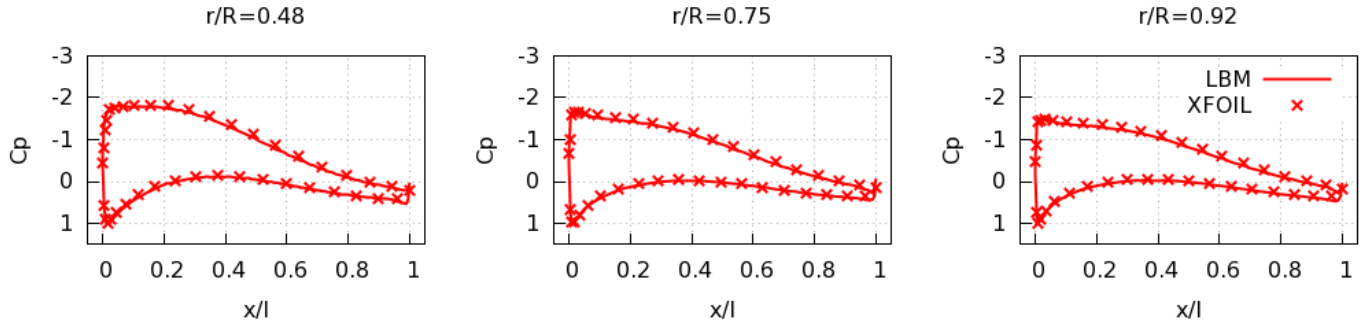

Fig. 4 Mean pressure distribution along different radial sections, integrated over multiple blades

different radial sections along the blade, the velocity magnitude in the rotating reference frame is plotted in Figure 5. It can be seen, first of all, that at all the three slices (locations according to Cp cuts from previous paragraph), a fully developed turbulent boundary has been formed thanks to the inclusion of the transition strip. At the inboard slice, at $r/R = 0.48$, the trailing edge is relatively thick and vortex shedding occurs. Traveling more outboard, the flow accelerates, the shedding diminishes, and the boundary layer becomes thinner.

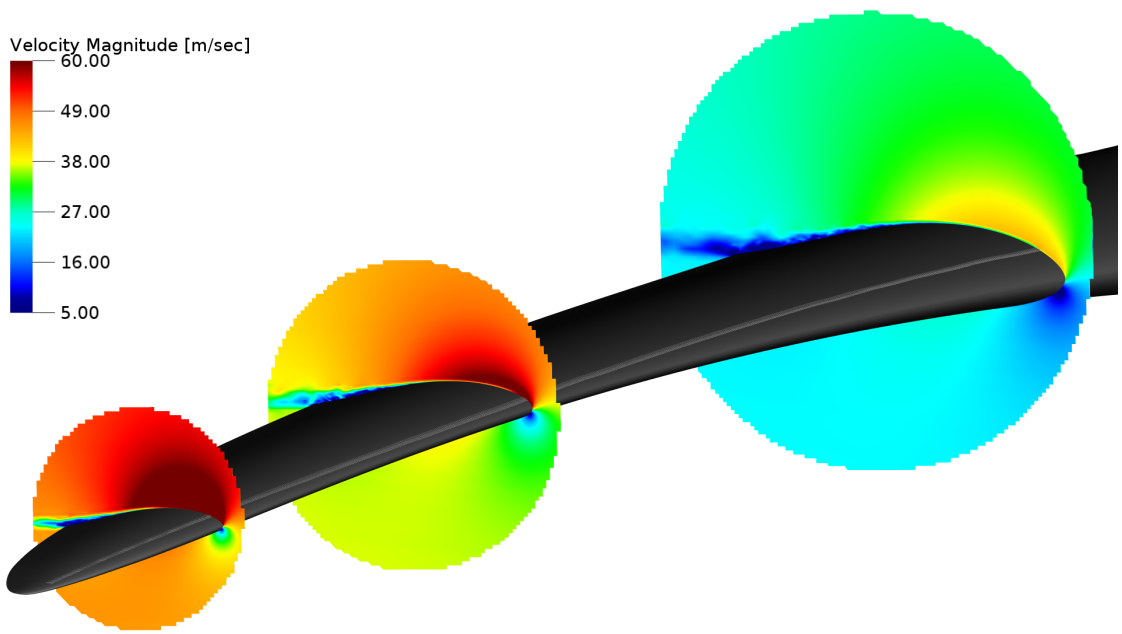

Fig. 5 Snapshot of the boundary layer development along the blade span

The indication of turbulence convecting over the trailing edge can be visualized by means of a dilation field, which is proportional to the time derivative of pressure. Snapshots of the suction (top) and pressure side (bottom) are shown in Figure 6. The result shows that, at outboard positions, a turbulent boundary layer is built up from the transition strip. Along the entire outboard trailing edge, strong levels of pressure variations are found, indicating the primary acoustic source location on this blade.

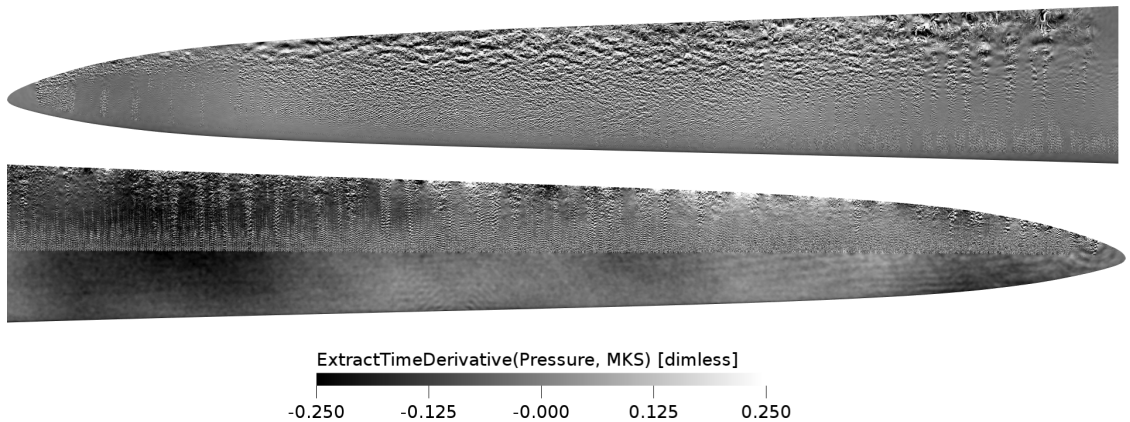

Fig. 6 Snapshot of time derivative of the pressure on the suction (top) and pressure (bottom) side

4.2. Certification noise analysis

The output of the acoustic certification prediction model involves various steps, which are described by their results in detail in this section. The unsteady surface pressure data, extracted from PowerFLOW, is the input into the model. Twelve physical ground microphones are used, distributed along a circle of 100 m radius around the turbine. In addition, a probe just 10 m away from the tower is used as another reference point. Each ground microphone is 72 times rotated along a coaxial ring, resulting in a total of 936 microphones at different positions.

The frequency-domain FW-H solver handles all these microphones, and calculate the resulting acoustic power spectral density using multiple Hanning windows. Ground reflection is taken into account already in this stage of the calculation. To indicate the spread obtained from different azimuthal probes (i.e. modulation due to blade rotation), the results of the downwind microphone is plotted in Figure 7, together with its Overall Sound Pressure Level (OASPL). Notice that these results come directly from the FW-H solver, and therefore correspond to the noise generated by one blade only, without Doppler effects. The large blue area is bounded by the minimum and maximum PSD obtained from all microphones. It indicates that, when calculating noise levels from slowly rotating blades, it is important to take into account the blade rotation with respect to the observer position, as the signal itself is very modulated over time. This is confirmed by observing the OASPL in Figure 7, as differences up to 15 dB are observed depending on microphone (and thus blade) angular position. Plotting in A-weighting scale yields similar variances between low and high level sound. This suggests that the swirling motion of the blades, at distances of 100 meter downwind from the tower, are still heavily been perceived by the observer.

When investigating a location closer to the tower, a stronger modulation of the source is expected. Indeed, when looking at Figure 8 (right), a variation between both locations is observed. Closer to the tower, the slanted distance is $\sqrt{100^2 + 60^2}/\sqrt{10^2 + 60^2} = 1.9$ times closer, and in generally slightly higher values in part of the revolution are observed. However, taking into account the distance variation, one would expect $20 \cdot \log_{10}(1.9) \approx 5.7$ dB, which is not observable for each single microphone on the right side of Figure 8. Instead, higher levels are observed for many of the 100 meter probes compared against the 10 meter azimuthal ground microphones. This means that, closer to the tower, the directivity effects of the isolated aerodynamic sources (e.g. trailing edge noise and tip noise) are

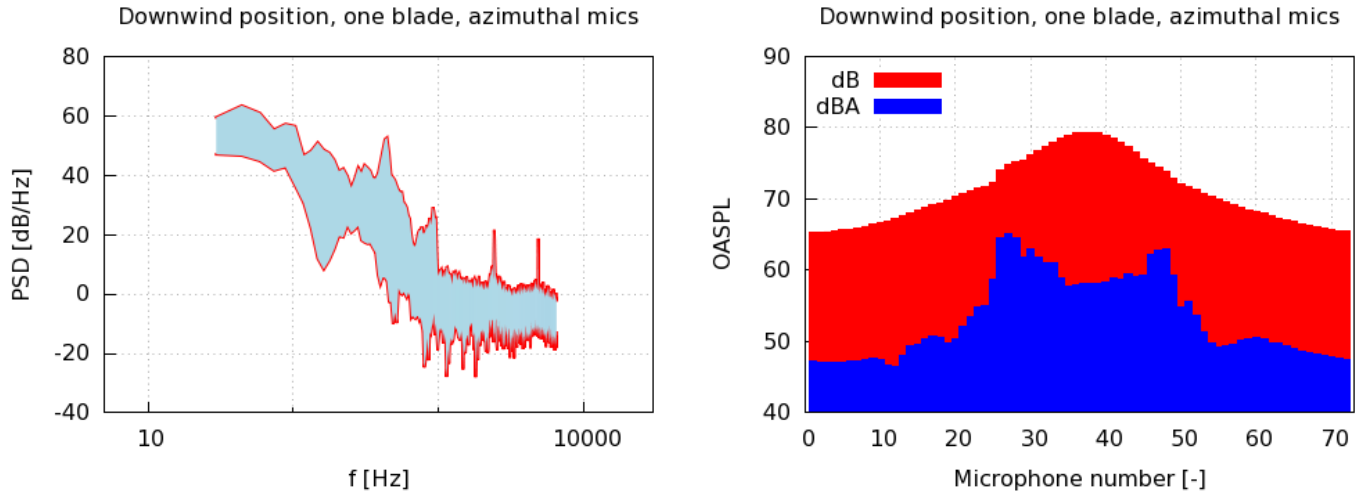

Fig. 7 FW-H PSD spectra (left) and OASPL (right) at all azimuthal locations for one downwind location

more pronounced. At a distance ten times further from the tower (the reference downwind position), the approximation of a point source can be made, and levels vary less over a revolution. This makes the variation of sound, and thus the swirling effect of a wind turbine, much more pronounced at locations close to the turbine, as shadow zones are more active. It can be seen that the variation at 100 meter is approximately 10 dB, while at 10 meter this increased to 35 dB.

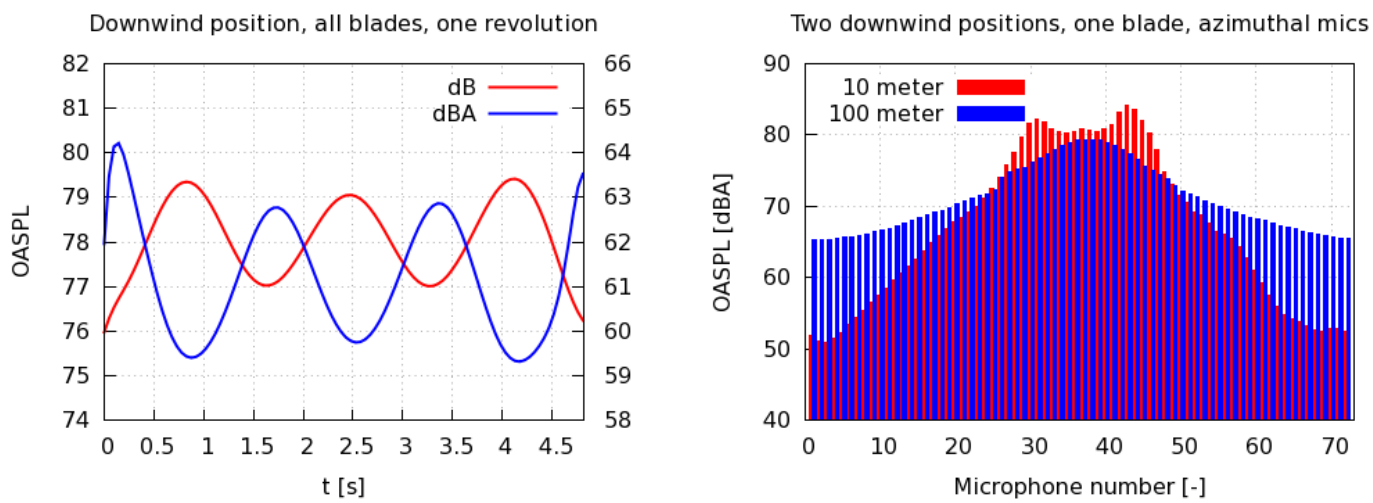

Fig. 8 Downwind position perceived OASPL in time (left) and for two downwind locations

Next step is to consider the full motion of the turbine, taking into account the three blades. Phase information is added to the computation, and one full revolution OASPL is depicted in Figure 8 (left). There is a shift of peak amplitude due to the A-weighting.

The final step in obtaining the certification apparent acoustic power (L_{WA}) and its spectrum, is to

generate a synthetic signal based on auralization, thereby also taking into account atmospheric absorption and Doppler effects. A total of 5 revolutions is reconstructed, and its L_{WA} is calculated using:

$$L_{WA} = L_V - 6 + 10 \cdot \log_{10} \left[\frac{4\pi \cdot R_1^2}{S_0} \right], \tag{1}$$

where L_V is the background corrected A-weighted sound pressure level, R_1 the slant distance in meters from the rotor center to the microphone and S_0 a reference area, for simplicity here set to unity. The result is depicted in Figure 9 (left) and can be considered to be the official downwind noise estimation according to IEC certification.

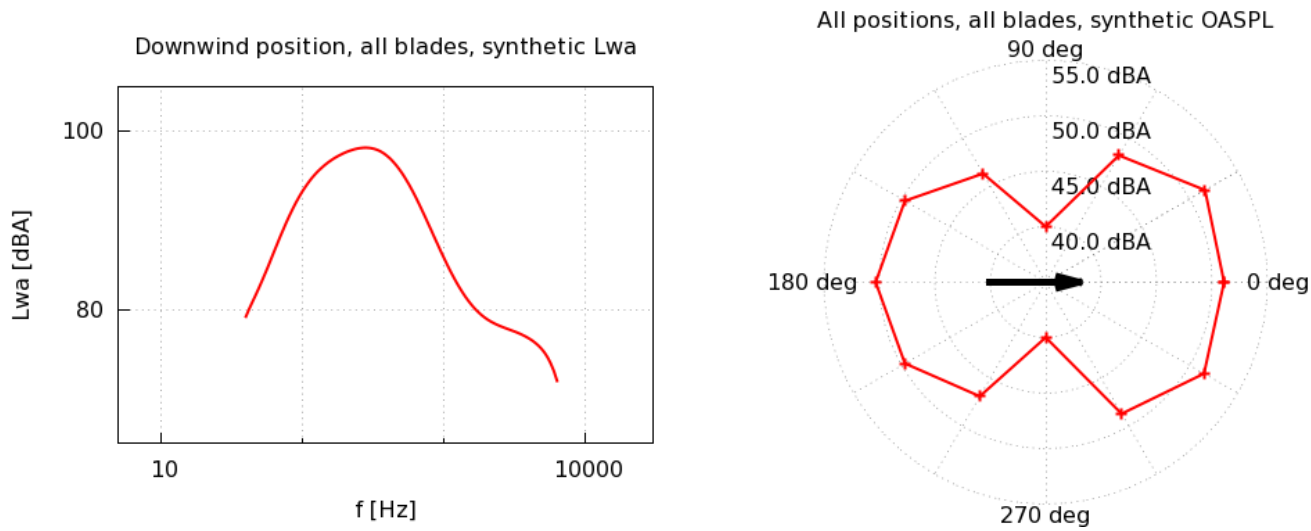

Fig. 9 Auralized apparant acoustic power Lwa (left) for the downwind position and its OASPL directivity (right)

Finally, the full process can be repeated for the other 11 physical ground microphones, oriented in a circle of 100 m radius around the turbine. The auralized OASPL is therefore plotted in a directivity pattern in Figure 9 (right). The wind direction is depicted by the arrow, and follows the positive x-axis along the default coordinate system. Zero degrees indicates the reference downwind position. The blade rotation is also oriented along the positive x-axis, meaning the down-stroke-going-blade is at the 270 degrees direction. From previous literature it is known that, when the observer is on the ground, the blade which convects its aerodynamic self-noise most efficiently, is the down-stroke-going blade [10]. The same is observed in the current computation, where OASPL levels at locations towards the 270 degrees angle are a few dB higher than at the 90 degrees location. A large shadow zone is present when standing in a side-wind position, while largest levels are seen in the downwind position.

5. Conclusion

Flow and acoustic simulations were performed on the NM80 full-scale 3-bladed wind-turbine, tested during the DanAero campaign. SIMULIA PowerFLOW's Lattice Boltzmann Method was used to predict the turbulent-resolved unsteady flow around the full wind-turbine, yielding good results with

reference XFOIL data. A fully turbulent boundary layer was observed at the outboard sections of the wing, making it possible in this study to digitally analyze turbulent boundary layer noise at full wind-turbine level.

The noise at certification position for five rotor revolutions was computed using an auralization technique from simulated flow data stored along a portion of the rotor revolution. The auralization process is based on a frequency-domain Ffowcs-Williams and Hawking noise spectrum computation from blade wall-pressure pressure fluctuations, taking into account ground reflection. Noise spectra at several azimuthal copies of the microphones were finally corrected to take into account blade-motion Doppler effects end atmospheric absorption and smoothly appended to recover the full rotor revolution.

Significant cost reduction in simulation time was found with the new post-processing process of determining certification noise levels according to IEC standards, making the entire process suitable for industrial turn-around-times. Furthermore, the new process allowed to investigate the physical insight of the noise propagation due to different microphone placements and frequency domain analysis, where similar conclusions as in other, experimental reference, papers were found.

Acknowledgments

The DanAero projects were funded partly by the Danish Energy Authorities, (EFP2007. Journal nr.: 33033-0074 and EUDP 2009-II. Journal nr.: 64009-0258) and partly by eigenfunding from the project partners Vestas, Siemens, LM, Dong Energy and DTU.

References

[1] Avallone, F., Casalino, D., and Ragni, D. (2018). Impingement of a propeller slipstream on a leading edge with a flow-permeable insert: A computational aeroacoustic study. *International Journal of Aeroacoustics*, 17(6-8).

[2] Brooks, T., Pope, D., and Marcolini, M. (1989). Airfoil self-noise and prediction. *NASA Technical Report, Reference Publication 1218*.

[3] Casalino, D., Avallone, F., Gonzalez-Martino, I., and Ragni, D. (2019). Aeroacoustic study of a wavy stator leading edge in a realistic fan/ogv stage. *Journal of Sound and Vibration*, 442:138–154.

[4] Casalino, D., Hazir, A., and Mann, A. (2018). Turbofan broadband noise prediction using the lattice boltzmann method. *AIAA Journal*, 56(2).

[5] Chen, H., Kandasamy, S., Orszag, S. A., Succi, S., and Yakhot, V. (2003). Extended boltzmann kinetic equation for turbulent flows. *Science*, 301(5633):633–636.

[6] Chen, H., Orszag, S., Staroselsky, I., and Succi, S. (2004). Expanded analogy between boltzmann kinetic theory of fluid and turbulence. *Journal of Fluid Mechanics*, 519:301–314.

[7] den Ende, L. V., Avallone, F., Casalino, D., Eitelberg, G., and L. L. M. V. (2018). Aerodynamic and aeroacoustic investigation of swirl recovery vanes for propeller propulsion systems. *31st Congress of the International Council of the Aeronautical Sciences, Belo Horizonte, Brazil,*, pages 1–19.

[8] Gonzalez-Martino, I. and Casalino, D. (2018). Fan tonal and broadband noise simulations at transonic operating conditions using lattice-boltzmann methods. *AIAA Paper 2018-3919*.

[9] Madsen, H., Bak, C., Paulsen, U., Gaunaa, M., Fuglsang, P., Romblad, J., Olesen, N., Enevoldsen, P., Laursen, J., and Jensen, L. (2010). The danaero experiments final report. Technical report, RISO-R-1726 (EN), Technical University of Denmark.

[10] Oerlemans, S., Sijtsma, P., and Lopez, B. M. (2006). Local and quantification of noise sources on a wind turbine. *Journal of Sound and Vibration*, 299:869–883.

[11] Pérot, F., Kim, M.-S., Meskine, M., and Freed, D. (2012). Nrel wind turbine aerodynamic validation and noise predictions using lbm. *AIAA Paper 2012-2287*.

[12] Romani, G. and Casalino, D. (2017). Application of lattice-boltzmann method to rotorcraft aerodynamics and aeroacoustics. In *Proceedings of the 43rd European Rotorcraft Forum, Milan, Italy*.

[13] van den Berg, F., Pedersen, F., Bouma, J., and Bakker, R. (2008). Windfarm perception: Visual and acoustic impact of wind turbine farms on residents. *University of Groningen*.

[14] Yakhot, V. and Orszag, S. A. (1986). Renormalization group analysis of turbulence. i. basic theory. *Journal of Scientific Computing*, 1(1):3–51.

[15] Yakhot, V., Orszag, S. A., Thangam, S., Gatski, T. B., and Speziale, C. G. (1992). Development of turbulence models for shear flows by a double expansion technique. *Physics of Fluids A*, 4(7):1510–1520.